Massachusetts Institute of Technology

Chemical Kinetics Mechanism for Oxy-Fuel Combustion of Mixtures of Hydrogen Sulfide and Methane

Dominik Bongartz, Ahmed F. Ghoniem*

Department of Mechanical Engineering, Massachusetts Institute of Technology, 77 Massachusetts Avenue, Cambridge, MA 02139, USA

Abstract

Oxy-fuel combustion of sour gas, a mixture of natural gas (essentially methane (CH_4)), carbon dioxide (CO_2), and hydrogen sulfide (H_2S), could enable the utilization of large natural gas resources, especially when combined with enhanced oil recovery. In this work, a detailed chemical reaction mechanism for oxy-fuel combustion of sour gas is presented. To construct the mechanism, a CH_4 sub-mechanism was chosen based on a comparative validation study for oxy-fuel combustion. This mechanism was combined with a mechanism for H_2S oxidation, and the sulfur sub-mechanism was then optimized to give better agreement with relevant experiments. The optimization targets included predictions for the laminar burning velocity, ignition delay time, and pyrolysis of H_2S, and H_2S oxidation in a flow reactor. The rate parameters of 15 sulfur reactions were varied in the optimization within their respective uncertainties. The optimized combined mechanism was validated against a larger set of experimental data over a wide range of conditions for oxidation of H_2S and interactions between carbon and sulfur species. Improved overall agreement was achieved through the optimization and all important trends were captured in the modeling results. The optimized mechanism can be used to make qualitative and some quantitative predictions on the combustion behavior of sour gas. The remaining discrepancies highlight the current uncertainties in sulfur chemistry and underline the need for more accurate direct determination of several important rate constants as well as more validation data.

Keywords: Sour gas, Sulfur, Hydrogen sulfide, Methane, Oxy-fuel, Kinetic modeling

1. Introduction

A large fraction of the world wide natural gas resources is currently not usable because it consists of 'sour' natural gas, or sour gas [1]. Unlike regular 'sweet' natural gas, which is made up mainly of methane (CH_4) and some other light hydrocarbons, sour gas also contains large amounts of hydrogen sulfide (H_2S) and carbon dioxide (CO_2). Depending on the gas field, the volume fractions of these contaminants often vary between zero and 30% each [2]. Both substances are undesirable; H_2S is toxic and its combustion products (especially sulfur trioxide (SO_3)) can cause severe corrosion problems, while CO_2 lowers the heating value of the gas. If the concentrations of H_2S and CO_2 get too high, expensive purification processes are necessary if the natural gas is to be used in a conventional gas fired power plant, which can make the use of the gas uneconomic.

Oxy-fuel combustion may provide a solution to this problem. In oxy-fuel combustion, the fuel is burned in pure oxygen (O_2) and some diluent (usually either CO_2, water (H_2O), or a mixture of these) instead of air. This yields combustion products consisting mainly of CO_2 and H_2O, which allows for easy separation of CO_2 by condensation of H_2O and makes oxy-fuel combustion an option for carbon capture and sequestration [3, 4]. Since the production of O_2 is energy intensive, oxy-fuel systems are likely to operate close to stoichiometry (equivalence ratio $\Phi \approx 1$) to

---

*Corresponding author. 77 Massachusetts Avenue, Room 3-344, Cambridge MA 02139, USA. Fax: +1-617-253-5981.
Email addresses: dominikb@mit.edu (Dominik Bongartz), ghoniem@mit.edu (Ahmed F. Ghoniem)

avoid wasting either fuel or energy for air separation. Thus, the combustion temperature is controlled by adjusting the amount of diluent that is added to the combustor.

In the case of sour gas, the problem of the low heating value can therefore be overcome when employing an oxy-fired combustion strategy by recycling less diluent to the combustor. Furthermore, the fact that oxy-fuel systems operate close to stoichiometry might alleviate corrosion issues associated with sulfur-containing combustion products. If the carbon dioxide produced in the oxy-fuel process is used for enhanced oil recovery (EOR), an additional revenue stream can be generated to counteract the higher cost and complexity of the process [5]. However, the use in EOR also gives rise to different requirements for the combustion products, one important change being that the O_2 content has to be limited to ppm levels [6].

To investigate the potential of this approach, it is necessary to characterize the combustion behavior of sour gas and in particular its chemical kinetics. We therefore need a detailed chemistry model that can capture most of the phenomena that arise from the unusual fuel and combustion environment. Eventually, such a model can also serve as a basis for the development of a reduced mechanism suitable for use in multi-dimensional computational fluid dynamics (CFD) simulations. Specifically, a good model should fulfill the following requirements:

- Capture the effects of CO_2 or H_2O diluted oxy-fuel conditions on the laminar burning velocity and the ignition delay time of CH_4 over a range of temperatures.

- Predict the formation and consumption of carbon monoxide (CO) and O_2 under oxy-fuel conditions with reasonable accuracy.

- Give accurate predictions for the laminar burning velocity and ignition delay time of H_2S over a range of temperatures and for different diluents.

- Predict the formation of SO_3 under the conditions of interest.

- Capture possible interactions between carbon and sulfur species and reproduce the correct relative oxidation speed of CH_4 and H_2S.

The purpose of this paper is to assemble and optimize a detailed chemical reaction mechanism for sour gas combustion that fulfills these requirements. We first present a comparative study of mechanisms for oxy-fuel combustion of CH_4 to identify a suitable CH_4 sub-mechanism. Next, we describe how this CH_4 mechanism was combined with a mechanism for the oxidation of H_2S and explain our optimization of the sulfur kinetics. Finally, we give a summary of the performance of the combined mechanism against experimental data (including but not limited to the optimization targets) on sulfur oxidation and interactions between CH_4 and H_2S.

2. Mechanism for Oxy-Fuel Combustion of CH_4

While there has been a considerable amount of work on modeling combustion of CH_4 in air, so far only few reaction mechanisms have been developed or at least tested specifically for the special conditions that are typical in oxy-fuel combustion (that is combustion close to stoichiometry in the presence of large fractions of CO_2 or H_2O). This group of mechanisms includes the GRI-Mech 3.0 [7], the mechanism developed by Glarborg et al. [8–10], and the mechanism developed by Dagaut et al. [11, 12]. However, to our knowledge there has been no comprehensive comparative study yet to show how well these mechanisms capture the effects caused by the unusual combustion environment.

In our case, the O-H subset of the mechanism is particularly important since it will also be used by the sulfur part of the mechanism (see Section 3). Therefore, we also included the AramcoMech 1.3 mechanism by Metcalfe et al. [13] in our study, since it is based on a recent O-H model [14] which (unlike the older mechanisms mentioned above) inludes the latest advances in this area, such as, for example, the improved rate constant for the reaction $H + O_2 = OH + O$ [15]. It should be noted that AramcoMech 1.3 does not contain a model for formation of nitrogen oxides (NOx). However this is not expected to be a major problem when dealing with oxy-fuel combustion, since a number of studies have found NOx formation to be negligible for realistic O_2 purities [16–18].

Several studies have shown that adding CO_2 to CH_4-air flames reduces the laminar burning velocity of CH_4 through both thermal and chemical effects [19–21]. The extent of this reduction is captured correctly by all three

tested mechanisms (see Fig. 1). For the mechanism by Dagaut et al., we encountered numerical difficulties for all burning velocity calculations.

There have been a number of studies on the impact of H_2O on the burning velocity of CH_4 [22–25]. While all three tested mechanisms can predict the decrease of the burning velocity through H_2O addition equally well at atmospheric pressure, AramcoMech 1.3 performs better at elevated pressure (see Fig. 2).

Levy et al. [26] measured the ignition delay time of CH_4 in different diluents and found that neither CO_2 nor H_2O have a significant effect. All four mechanisms considered here agree reasonably well with their measurements in mixtures containing CO_2 (see Fig. 3a) and both CO_2 and H_2O (see Fig. 3b).

Recently, the influence of CO_2 and H_2O on CO oxidation has been investigated by several researchers (e.g., [12, 27]). Our tests showed that all four mechanisms are able to reproduce the inhibiting effect of large CO_2 concentrations on CO oxidation observed by Abián et al. [27] both for lean and rich conditions (see Fig. 4; only the case with the highest CO_2 content is shown here for better readability). The experimental data is best reproduced by GRI-Mech 3.0. The Glarborg mechanism predicts the onset of CO oxidation to be at slightly lower temperatures than what is observed experimentally.

The enhancing effect of moderate concentrations of H_2O on CO oxidation in the presence of CO_2 in the same experiment is captured qualitatively by all mechanisms (see Fig. 5; again, only the case with the highest H_2O content is shown). The inhibiting effect of larger concentrations of H_2O on CO oxidation at very lean conditions ($\Phi \approx 0.04$) observed by Glarborg et al. [28] is also captured by all models (see Fig. 6). In both cases, the Glarborg mechanism again predicts lower temperatures for the onset of CO oxidation.

While previous cases studied the impact of CO_2 and H_2O on CO oxidation, all mechanisms can at least qualitatively predict the effect of CO_2 on CO concentrations in CH_4 oxidation in the experiment of Glarborg and Bentzen [8] (see Fig. 7). At stoichiometric and fuel-rich conditions, the temperature above which increased CO is observed is best predicted by AramcoMech 1.3 and the Dagaut mechanism.

In summary, AramcoMech 1.3 provides the best overall agreement with the experimental data in the presented relevant validation cases, especially for the burning velocity at elevated pressure and CO formation in CH_4 oxidation. Based on this observation and the fact that it contains the most recent O-H submodel of the mechanisms considered here, we selected it as the basis for our mechanism for sour gas combustion.

3. Mechanism for H_2S Oxidation

To construct a mechanism for sour gas combustion, we chose to combine AramcoMech 1.3 (including its O-H submodel) with a suitable mechanism for H_2S oxidation. However, testing this basic combined reaction mechanism revealed discrepancies between experiment and modeling for important combustion parameters of H_2S such as laminar burning velocity and ignition delay time. This motivated the tuning of the sulfur mechanism to improve the agreement with experiments under relevant conditions. In this section, we first describe the selection of the H_2S mechanism and the optimization procedure. Next, we present the performance of the mechanism for the optimization targets as well as other experiments.

3.1. Mechanism Selection and Optimization

Sulfur oxidation chemistry is far less well established than hydrocarbon chemistry, but there has been a growing interest in the topic in recent years and a number of detailed reaction mechanisms have been proposed, including the work of Frenklach et al. [29]; Glarborg et al. [30]; Alzueta et al. [31]; the Leeds sulfur mechanism [32], and the mechanism presented by Cerru et al. [33, 34]. Recently, Zhou et al. [35] presented a mechanism for H_2S oxidation that puts more emphasis on the chemistry of disulfur species. Since these were found to be particularly important near stoichiometric conditions, this mechanism was chosen as the basic sulfur mechanism.

Only the reactions containing sulfur-species were adopted from the mechanism of Zhou et al., since the O-H reactions are already contained in AramcoMech 1.3. These reactions that determine the O-H radical pool are important for both CH_4 and H_2S oxidation and hence provide a means of interaction between the two fuels. The mechanism does not include any species containing both carbon and sulfur such as carbonyl sulfide (COS) or carbon disulfide (CS_2), the influence of which Cerru et al. [33] found to be negligible. The resulting combined mechanism consists of 157 species and 1011 reactions.

The thermodynamic data was taken from AramcoMech 1.3 and Zhou et al. [35], except for the enthalpy of formation of the mercapto radical (SH), which was set to $\Delta H_{f,298}^{0}(SH) = 33.8$ kcal/mol. This is in agreement with the recent recommendations of Goos et al. [36] and Denis [37] while improving overall agreement with the experimental data used for validation. Because of this change, we also had to adjust the rate parameters for the high-pressure limit of the reaction SH + SH (+M) = HSSH (+M) since they were originally determined from the backward reaction using the equilibrium constant, which is affected by the thermodynamic data [38]. The new rate constant is only about half of the original one and has a higher activation energy.

As mentioned above, there where some important experiments for which significant discrepancies were observed between the experimental data and the modeling results with this initial combined mechanism. To improve the overall performance of the mechanism, the following cases were chosen as targets in a systematic optimization of the sulfur kinetics:

- the laminar burning velocity of H_2S in air at atmospheric pressure [39–42]

- the ignition delay time of H_2S in air as measured by Frenklach et al. [29]

- the pyrolysis of H_2S in the experiment of Hawboldt et al. [43]

- the H_2S flow reactor experiment of Zhou et al. [35]

The exact points used, the corresponding target values, and the assigned weights are listed in Table 1. For the laminar burning velocity (target 1), a target range was chosen to account for the scatter of the data points from the different experiments. For the ignition delay time (targets 2–5), target ranges were chosen because the selection of a single data point led to arbitrarily different results. For the flow reactor experiment of Zhou et al. [35], we only considered the cases with an equivalence ratio of $\Phi = 0.8$ (targets 8–12) because they are closer to the conditions around stoichiometry that occur in oxy-fuel combustion than the third case presented therein ($\Phi = 0.15$).

The objective function f used in the optimization was defined as the sum of the quadratic deviations of the modeling predictions (x_i) from the target values ($X_{i,min}$, $X_{i,max}$) normalized by a characteristic value ($X_{i,char}$), multiplied by the respective weights (w_i):

$$f = \sum_i w_i \cdot \frac{\frac{1}{4}\left[\text{sgn}(x_i - X_{i,min}) + \text{sgn}(x_i - X_{i,max})\right]^2 \cdot \min\left[(x_i - X_{i,min})^2, (x_i - X_{i,max})^2\right]}{X_{i,char}^2} \tag{1}$$

In most cases, $X_{i,char}$ was set to be the target value (or the mean of the upper and lower limit of the target range). However, for targets 10–12 a common value of 300 ppm was chosen in order to avoid a division by zero for target 12. In order to achieve good overall agreement, target 12 was therefore assigned an empirically determined increased weight. Increased weight was also assigned to the laminar burning velocity (target 1) due to its importance in characterizing the flame stabilization behavior of a fuel, also keeping in mind the intended future use of a reduced version of the mechanism for CFD of turbulent flames. The sum in Eq. (1) did not necessarily include all targets listed in Table 1, but different subsets were used to obtained different optimized versions of the mechanism by only considering certain combinations of experiments. In the comprehensive model validation presented in the next section, three of these versions were investigated. In the following, they are referred to as 'Optimization 1–12', 'Optimization 1–7', and 'Optimization 8–12', where the numbers are the target numbers given in Table 1. These combinations correspond to an optimization with respect to all experiments mentioned above, all experiments except the H_2S flow reactor of Zhou et al. [35], and only the H_2S flow reactor, respectively.

The decision variables used in the optimization were the pre-exponential factors for the rate constants of 15 reactions in the sulfur mechanism to which the results for the target cases were particularly sensitive. To identify these reactions, we conducted sensitivity analyses for targets 1–7. Sensitivity analyses for the flow reactor experiment (targets 8–12) were already conducted by Zhou et al. [35]. The results of some of these analyses are summarized in Fig. 8. The reactions highlighted in boldface (also listed in Table 2) were chosen to be varied in the systematic optimization of the mechanism. Note that these also include the ten reactions Zhou et al. [35] found to be the most important for their flow reactor experiment. We confirmed this in a similar analysis for the present combined model. For the pressure dependent reactions SH + SH (+M) = HSSH (+M) and H + SO$_2$ (+M) = HOSO (+M), the rate

constants for both high and low pressure limit were considered. For the reaction $H_2S + S$ (+M) = HSSH (+M), only the high pressure expression was included as a decision variable, since even at atmospheric pressure the reaction is almost in the high-pressure limit [38]. Thus, a total of 17 decision variables were used in the optimization. The large number of reactions that had to be varied to improve the agreement with the different experiments simultaneously is a first indication of the significant uncertainties remaining in sulfur chemistry. An earlier attempt considering only 10 of the present 15 reactions was significantly less successful.

The constraints on the variations of the decision variables were determined from the uncertainties reported for the original experiments or calculations wherever possible, to make sure that the values for the rate parameters determined through the optimization are still in agreement with the more direct experimental or theoretical determinations. For the reaction $S + O_2 = SO + O$, the uncertainty of the pre-exponential factor was determined as +50%/-20% by comparison with the experimental data used in the original fitting by Lu et al. [44]. In a similar fashion, we determined the constraints on the variation of the pre-exponential factor of the reaction $H_2S + H = SH + H_2$ as ±25% by comparison with the experimental data used by Peng et al. [45]. For the reaction $SO + O_2 = SO_2 + O$, we reevaluated the fit to the experimental data of Grillo et al. [46], Black et al. [47], and Garland [48]. The uncertainty of the pre-exponential factor was determined to be about 10% by combining the higher and lower limits for the different rate constants considered in the fitting. For the reaction $H_2S + S = SH + SH$, two duplicate reactions corresponding to different reaction channels were defined in the original sulfur mechanism [35]. We determined the uncertainties in the pre-exponential factors of each of these by varying them and comparing the resulting fit to the original data of Gao et al. [49] and Shiina et al. [50]. The limits on the variation of the pre-exponential factor that were chosen are +20%/-40% for the first of the two duplicate reactions and ±25% for the second reaction. The rate expression for the reaction $H_2S + O = SH + OH$ used in the mechanism was determined from theoretical calculations, but the comparison with experimental data presented by Wang et al. [51] suggests an uncertainty of a factor of two. The rates of the other reactions were obtained from theoretical calculations alone so that an uncertainty of a factor of three was assumed [38, 52].

We implemented a simple coordinate descent method (see e.g. [53]) to solve the optimization problem described above, i.e. only one decision variable was varied at a time with the others being constant. This one-dimensional line search problem was solved with the golden section method. The calculations needed for evaluating the objective function were conducted using CHEMKIN-PRO [54]. Once an optimal value was found, the next variable was varied. The order in which the decision variables were optimized was chosen randomly at the beginning of each loop over the 17 decision variables. This procedure was repeated until the relative change in the objective function between two consecutive loops over all variables was negligible ($\leq 10^{-5}$). Typically, between 25 and 35 iterations over all decision variables were necessary to achieve a converged solution, taking between 10 and 50 hours of CPU time total, depending on the number of targets used.

Optimization with respect to the three different combinations of targets ('Optimization 1–12', 'Optimization 1–7', and 'Optimization 8–12') resulted in different values for the rate parameters that were varied (see Table 2). A complete version of the combined mechanism which was found to give the best overall agreement, 'Optimization 1–12' (see Section 3.2), is available as supplementary material.

For a number of reactions, the rates were changed in the opposite direction and the optimal values differ by almost a factor of ten depending on the combination of targets used. In particular, the reactions

$$H_2S + S = SH + SH$$
$$H + HSS = SH + SH$$
$$SH + SH(+M) = HSSH(+M)$$
$$S + SH = S_2 + H$$
$$H_2S + O = SH + OH$$
$$S + O_2 = SO + O$$
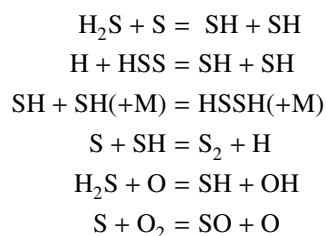
show conflicting changes in the different optimized versions while having a strong influence on the results, and thus require a more accurate direct determination of their rate constants to resolve the current uncertainties.

3.2. Mechanism Performance

To demonstrate the performance of the combined mechanism, we first present the results for the basic combined mechanism and the three optimized combined mechanisms ('Optimization 1–12', 'Optimization 1–7', and 'Optimization 8–12') in the cases that served as optimization targets. Next, we summarize additional validation cases for sulfur oxidation and interactions between carbon and sulfur species. Where possible, emphasis was put on situations that are relevant to oxy-fuel combustion. All modeling calculations were again conducted using CHEMKIN-PRO [54]. For cases in which the different optimized versions led to different results, the calculations with all four mechanisms are shown. In all other cases, only the computation using the recommended version 'Optimization 1–12' is presented.

3.2.1. Optimization Targets

To our knowledge, the laminar burning velocity of H_2S in air (target 1) has been measured in only four studies [39–42] and there is considerable scatter in the data. However, at soichiometric conditions (which are most important for the intended application) most experiments suggest a value around 40 cm/s (see Fig. 9), meaning that the prediction of the basic combined mechanism is too high. We found that this discrepancy could be removed by considering the laminar burning velocity as a target in the optimization.

Frenklach et al. [29] measured the ignition delay time of H_2S in air at pressures of p = 30-45 bar under fuel-lean and fuel-rich conditions (targets 2–5). For our modeling, the ignition delay time was taken to be the time needed for a temperature rise of ΔT = 600 K similar to [34], but the results were found to be not sensitive to the exact definition. Figure 10 shows that while the calculated order of magnitude is correct, the temperature dependence predicted by the basic mechanism is somewhat too strong. Again, improved agreement was achieved in the optimization, especially if targets 8–12 were not used.

Zhou et al. [35] also presented data on lean H_2S oxidation in an atmospheric flow reactor (targets 8–12). Figure 11 shows that while the trends of the prediction with the basic mechanism for the H_2S profiles are correct, the profiles are shifted to lower temperatures, which is in agreement with the original findings of Zhou et al. This could be improved by including the experiment as an optimization target. If the optimization was conducted only against the other 7 targets, the predicted conversion is much too low. The prediction quality for sulfur dioxide (SO_2) is comparable to the H_2S profiles (see Fig. 12). Hydrogen is overpredicted (see Fig. 13), in agreement with the results of Zhou et al.

The pyrolysis of H_2S has been the subject of a number of experimental (e.g., [43, 55]) and modeling (e.g., [50, 52]) studies. Compared to the experimental data of Hawboldt et al. [43] (targets 6–7), H_2S conversion predicted by the basic mechanism tends to be too slow for most temperatures (see Fig. 14). The optimization was able to improve this if the experiment was used as a target, but even optimization only against the flow reactor of Zhou et al. [35] led to some improvements.

3.2.2. Validation: H_2S Oxidation

Very recently, Mathieu et al. [56] measured the ignition delay time of H_2/H_2S mixtures. The basic combined mechanism predicts a shorter ignition delay than measured at high temperature, while at p = 33 atm and low temperature there is a change in the slope of the Arrhenius plot that is not observed experimentally (see Fig. 15). The agreement is improved only for the version of the mechanism (Optimization 1–7) that was optimized against all targets except for the flow reactor of Zhou et al. This is consistent with the observation in the experiment of Frenklach et al. [29] (cf. Fig. 10) and highlights the difficulty of reconciling the flow reactor data and the ignition delay time. This was also observed by Mathieu et al. [56], who were able to manually tune the same basic mechanism (the sulfur mechanism of Zhou et al. [35] and the H_2 mechanism of Kéromnès et al. [14]) to give even better agreement for their own data than the present model, but at the expense of deteriorated predictions for the flow reactor [35] and also for H_2S pyrolysis in the experiment of Hawboldt et al. [43]. Including the experiment of Mathieu et al. [56] as an optimization target did not improve the overall agreement or clarify the conflicting trends in the reaction rates (cf. Table 2).

Merryman and Levy [57] measured the flame structures of premixed H_2S flames at low pressure. Figure 16 shows that the prediction of the major species is good while the hydrogen (H_2) concentration is somewhat overpredicted, similar to the flow reactor results mentioned above. The predictions with the different optimized versions are virtually identical.

While the primary combustion product of H_2S is SO_2, some SO_3 can be formed during cooling of the flue gas by further oxidation of SO_2 in the presence of excess O_2. This is a major concern due to the role of SO_3 in sulfuric

acid corrosion and low temperature hot corrosion [58–60]. The formation of SO_3 has been predicted to be increased in oxy-coal combustion compared to air combustion [61], mainly because SO_2 is recycled with the flue gas, thus leading to a higher sulfur concentration. However, this can be overcome by appropriate cycle design. Additional improvements are expected for oxy-fuel combustion of gaseous fuels, since gas-fired plants can operate much closer to stoichiometric conditions which reduces the excess O_2 that is needed for SO_3 formation.

Fleig et al. [62] recently investigated the formation of SO_3 in a flow reactor over a wide range of conditions. Figure 17 shows a comparison of the modeling results with some of their experimental data. It can be seen that the mechanism can capture the qualitative changes with varying O_2 and SO_2 content, the influence of an environment with high CO_2 concentration, and the impact of H_2O. However, there remain some quantitative discrepancies, especially at higher temperatures. This was also observed by Fleig et al. [62] using the kinetic model from [63]. We were not able to remove this discrepancy by including these experiments as optimization targets.

3.2.3. Validation: Interactions Between CH_4 and H_2S

One possible interaction between carbon and sulfur species is the inhibition of CO oxidation by SO_2 [30, 31, 63, 64]. The combined mechanism can capture the inhibiting effect of SO_2 on CO oxidation at stoichiometric conditions observed by Giménez-López et al. [63] both in a nitrogen (N_2) bath and in the presence of CO_2 (see Fig. 18). Comparable agreement is achieved for the flow reactor experiment of Dagaut et al. [64]. The different optimized versions lead to slight variations of the predicted profiles for the case with SO_2, but the overall quality of the prediction is not altered significantly.

Chin et al. [65] measured the simultaneous oxidation of CH_4 and H_2S in a flow reactor under fuel-rich conditions. As can be seen from Fig. 19, the combined mechanism can predict the relative oxidation speed of the two fuels, although there are some quantitative discrepancies especially for methane.

Fleig et al. [62] also investigated the influence of CO and CH_4 on the oxidation of SO_2 to SO_3. As shown in Fig. 20, the model qualitatively predicts the increased SO_3 formation at intermediate temperatures in the presence of combustibles. The slightly varying extent of this effect when comparing different amounts of CO/CH_4 is not captured correctly.

4. Conclusion

A detailed chemical kinetic model has been developed for oxy-fuel combustion of sour gas by combining existing mechanisms for CH_4 and H_2S and optimizing the sulfur kinetics:

1. A comparative study of mechanisms for oxy-fuel combustion of CH_4 showed that current mechanisms give good agreement with the experiment for the impact of the typical oxy-fuel diluents on the laminar burning velocity, ignition delay time, and CO concentrations.
2. AramcoMech 1.3 was chosen as the CH_4 sub-mechanism for the combined model because of its good performance at elevated pressure and its new O-H model.
3. The sulfur part of the mechanism was optimized by varying the rate parameters of 15 reactions within the experimental or computational uncertainties. While it was possible to get good agreement for a combination of the laminar burning velocity, ignition delay time, and pyrolysis data or for the H_2S flow reactor data [35], the discrepancies were larger if a combination of those two groups was considered. For the recommended version ('Optimization 1–12'), overall agreement for the oxidation of H_2S and formation of SO_3 after optimization is reasonable.
4. The mechanism can also predict phenomena related to the interaction between carbon and sulfur species. The predicted relative oxidation speed of CH_4 and H_2S is correct.
5. Some quantitative discrepancies remain that highlight the uncertainties that still exist in sulfur chemistry. In particular, the rates of several important reactions were changed in opposite directions in the optimization, depending on which targets were used. This underlines the need for more accurate direct determination of their rate constant.
6. We also observe that the amount of experimental data on sulfur combustion chemistry that is available for validation is very limited. More reliable data on laminar burning velocities and flame structures for H_2S, especially at higher pressure, as well as data on CH_4/H_2S flames under air and oxy-fuel conditions would be extremely valuable in this respect.

Acknowledgments

References

[1] W. F. J. Burgers, P. S. Northrop, H. S. Kheshgi, J. A. Valencia, Energy Procedia 4 (2011) 2178–2184.

[2] G. Hammer, T. Lübcke, R. Kettner, M. R. Pillarella, H. Recknagel, A. Commichau, H.-J. Neumann, B. Paczynska-Lahme, in: Ullmann's Encyclopedia of Industrial Chemistry, volume 23, Wiley-VCH, Weinheim, 2012, p. 740.

[3] M. B. Toftegaard, J. Brix, P. A. Jensen, P. Glarborg, A. D. Jensen, Prog. Energ. Combust. Sci. 36 (2010) 581–625.

[4] H. M. Kvamsdal, K. Jordal, O. Bolland, Energy 32 (2007) 10–24.

[5] J. Davison, Energy 32 (2007) 1163–1176.

[6] G. Pipitone, O. Bolland, Int. J. Greenh. Gas Con. 3 (2009) 528–534.

[7] G. P. Smith, D. M. Golden, M. Frenklach, N. W. Moriarty, B. Eiteneer, M. Goldenberg, C. T. Bowman, R. K. Hanson, S. Song, W. C. Gardiner, Jr., V. V. Lissianski, Z. Qin, GRI-Mech 3.0, available at http://www.me.berkeley.edu/gri-mech/version30/text30.html.

[8] P. Glarborg, L. L. B. Bentzen, Energy Fuels 22 (2008) 291–296.

[9] T. Mendiara, P. Glarborg, Combust. Flame 156 (10) (2009) 1937–1949.

[10] Z. Tian, Y. Li, L.Zhang, P. Glarborg, F. Qi, Combust. Flame 156 (2009) 1413 – 1426.

[11] T. Le Cong, P. Dagaut, G. Dayma, J. Eng. Gas Turb. Power 130 (2008) 041502.

[12] T. Le Cong, P. Dagaut, Energy Fuels 23 (2009) 725–734.

[13] W. K. Metcalfe, S. M. Burke, S. S. Ahmed, H. J. Curran, Int. J. Chem. Kinet. 45 (2013) 638–675.

[14] A. Keromnes, W. K. Metcalfe, K. A. Heufer, N. Donohoe, A. K. Das, C.-J. Sung, J. Herzler, C. Naumann, P. Griebel, O. Mathieu, M. C. Krejci, E. L. Petersen, W. J. Pitz, H. J. Curran, Combust. Flame 160 (2013) 995–1011.

[15] Z. Hong, D. F. Davidson, R. K. Hanson, Combust. Flame 158 (2011) 633 – 644.

[16] G. Richards, K. Casleton, B. Chorpening, Proc. Inst. Mech. Eng. A J. Power Energy 219 (2005) 121–126.

[17] T. Williams, C. Shaddix, R. Schefer, Combust. Sci. Technol. 180 (2008) 64–88.

[18] R. Lewis, K. Caselton, G. Richards, D. Straub, W. Rogers, in: 2001 Joint International Combustion Symposium, Kauai, HI.

[19] F. Liu, H. Guo, G. J. Smallwood, Combust. Flame 133 (4) (2003) 495–497.

[20] F. Halter, F. Foucher, L. Landry, C. Mounaïm-Rousselle, Combust. Sci. Technol. 181 (6) (2009) 813–827.

[21] V. R. Kishore, N. Duhan, M. R. Ravi, A. Ray, Exp. Therm. Fluid Sci. 33 (2008) 10–16.

[22] E. Albin, H. Nawroth, S. Göke, Y. D'Angelo, C. Paschereit, Fuel Process. Technol. 107 (2013) 27–35.

[23] A. N. Mazas, B. Fiorina, D. A. Lacoste, T. Schuller, Combust. Flame 158 (12) (2011) 2428–2440.

[24] V. Babkin, A. V'yun, Combust. Explos. Shock Waves 7 (1971) 339–341.

[25] T. Le Cong, P. Dagaut, in: Proceedings of ASME Turbo Expo 2008, pp. GT2008–50272.

[26] Y. Levy, E. Olchanski, V. Sherbaum, V. Erenburg, A. Burcat, J. Propul. Power 22 (3) (2006) 669–676.

[27] M. Abián, J. Giménez-López, R. Bilbao, M. U. Alzueta, Proc. Combust. Inst. 33 (2011) 317–323.

[28] P. Glarborg, D. Kubel, P. G. Kristensen, J. Hansen, K. Dam-Johansen, Combust. Sci. Technol. 110-111 (1) (1995) 461–485.

[29] M. Frenklach, J. H. Lee, J. N. White, W. C. Gardiner, Jr., Combust. Flame 41 (1981) 1–16.

[30] P. Glarborg, D. Kubel, K. Dam-Johansen, H.-M. Chiang, J. W. Bozzelli, Int. J. Chem. Kinet. 28 (1996) 773–790.

[31] M. U. Alzueta, R. Bilbao, P. Glarborg, Combust. Flame 127 (4) (2001) 2234–2251.

[32] Leeds University, The SOx mechanism extension to the Leeds Methane Oxidation Mechanism, available at http://garfield.chem.elte.hu/Combustion/Combustion.html.

[33] F. G. Cerru, A. Kronenburg, R. P. Lindstedt, Proc. Combust. Inst. 30 (2005) 1227–1235.

[34] F. G. Cerru, A. Kronenburg, R. P. Lindstedt, Combust. Flame 146 (3) (2006) 437–455.

[35] C. Zhou, K. Sendt, B. S. Haynes, Proc. Combust. Inst. 34 (2013) 625–632.

[36] E. Goos, A. Burcat, B. Ruscic, Ideal gas thermochemical database with updates from active thermochemical tables, available at http://garfield.chem.elte.hu/Burcat/burcat.html, 2013.

[37] P. A. Denis, J. Sulfur Chem. 29 (3-4) (2008) 327–352.

[38] C. Zhou, K. Sendt, B. S. Haynes, J. Phys. Chem. A 113 (2009) 8299–8306.

[39] D. S. Chamberlin, D. R. Clarke, Ind. Eng. Chem. 20 (10) (1928) 1016–1019.

[40] L. Cohen, Fuel 34 (1955) S119–S122.

[41] G. J. Gibbs, H. F. Calcote, J. Chem. Eng. Data 4 (3) (1959) 226–237.

[42] C. Flockenhaus, Gas Wärme Int. 18 (4) (1969) 153–156.

[43] K. A. Hawboldt, W. D. Monnery, W. Y. Svrcek, Chem. Eng. Sci. 55 (2000) 957–966.

[44] C.-W. Lu, Y.-J. Wu, Y.-P. Lee, R. S. Zhu, M. C. Lin, J. Chem. Phys. 121 (17) (2004) 8271–8278.

[45] J. Peng, X. Hu, P. Marshall, J. Phys. Chem. A 103 (1999) 5307–5311.

[46] A. Grillo, R. Reed, M. W. Slack, in: Proceedings of the 12th International Symposium on Shock Tubes and Waves, Jerusalem, July 12-19, 1979, Magnes Press, The Hebrew University, 1980, pp. 486–494.

[47] G. Black, R. L. Sharpless, T. G. Slanger, Chem. Phys. Lett. 93 (6) (1982) 598–602.

[48] N. L. Garland, Chem. Phys. Lett. 290 (1998) 385–390.

[49] Y. Gao, C. Zhou, K. Sendt, B. S. Haynes, P. Marshall, Proc. Combust. Inst. 33 (2011) 459–465.

[50] H. Shiina, M. Oya, K. Yamashita, A. Miyoshi, H. Matsui, J. Phys. Chem. 100 (6) (1996) 2136–2140.

[51] C. Wang, G. Zhang, Z. Wang, Q. S. Li, Y. Zhang, J. Mol. Struct.-THEOCHEM 731 (2005) 187–192.

[52] K. Sendt, M. Jazbec, B. S. Haynes, Proc. Combust. Inst. 29 (2002) 2439–2446.

[53] D. Bertsekas, Nonlinear Programming, Athena Scientific, 2nd edition, 1999.

[54] R. J. Kee, F. M. Rupley, J. A. Miller, et al., CHEMKIN-PRO 15112, Reaction Design, San Diego, CA, 2011.

[55] M. Binoist, B. Labégorre, F. Monnet, P. D. Clark, N. I. Dowling, M. Huang, D. Archambault, E. Plasari, P.-M. Marquaire, Ind. Eng. Chem. Res. 42 (2003) 3943–3951.

[56] O. Mathieu, F. Deguillaume, E. L. Petersen, Combust. Flame 161 (1) (2014) 23–36.

[57] E. L. Merryman, A. Levy, J. Air Pollut. Control Assoc. 17 (12) (1967) 800–806.

[58] R. Stanger, T. Wall, Prog. Energ. Combust. Sci. 37 (2011) 69–88.

[59] G. Blythe, K. Dombrowski, SO_3 Mitigation Guide Update, Technical Report 1004168, EPRI, Palo Alto, CA, 2004.

[60] N. Eliaz, G. Shemesh, R. M. Latanision, Eng. Fail. Anal. 9 (2002) 31–43.

[61] D. Fleig, F. Normann, K. Andersson, F. Johnsson, B. Leckner, Energy Procedia 1 (2009) 383–390.

[62] D. Fleig, M. U. Alzueta, F. Normann, M. Abián, K. Andersson, F. Johnsson, Combust. Flame 160 (6) (2013) 1142–1151.

[63] J. Giménez-López, M. Martínez, A. Millera, R. Bilbao, M. U. Alzueta, Combust. Flame 158 (1) (2011) 48–56.

[64] P. Dagaut, F. Lecomte, J. Mieritz, P. Glarborg, Int. J. Chem. Kinet. 35 (2003) 564–575.

[65] H. S. F. Chin, K. Karan, A. K. Mehrotra, L. A. Behie, Can. J. Chem. Eng. 79 (2001) 482–490.

Tables

Table 1: Targets used in the optimization of the combined mechanism.

No.	Case	Point	Target Value	Weight	Reference
1	H_2S Laminar Burning Velocity	$\Phi = 1$	42-46 cm/s	40	[39–42]
2	H_2S Ignition Delay Time	$\Phi = 0.5$, $T = 950$ K	1000-1600 µs	1	[29]
3		$\Phi = 0.5$, $T = 1200$ K	60-90 µs	1	[29]
4		$\Phi = 1.8$, $T = 950$ K	1600-2500 µs	1	[29]
5		$\Phi = 1.8$, $T = 1200$ K	100-160 µs	1	[29]
6	H_2S Pyrolysis	$T = 1000$ °C, $t = 0.64$ s	18.6% H_2S Loss	1	[43]
7		$T = 1150$ °C, $t = 0.17$ s	45.1% H_2S Loss	1	[43]
8	H_2S Flow Reactor, 520 ppm	$T = 1000$ K	498 ppm H_2S	1	[35]
9		$T = 1050$ K	19 ppm H_2S	1	[35]
10	H_2S Flow Reactor, 325 ppm	$T = 1030$ K	314 ppm H_2S	1	[35]
11		$T = 1070$ K	132 ppm H_2S	1	[35]
12		$T = 1100$ K	0 ppm H_2S	10	[35]

Table 2: Changes in the pre-exponential factors relative to the values in [35] for optimization against different target combinations.

Reaction	Optimization 1–12	Optimization 1–7	Optimization 8–12
$H_2S + H = SH + H_2$	0.96	3.00	0.33
$H_2S + S = SH + SH$ (1)	1.20	0.83	1.00
$H_2S + S = SH + SH$ (2)	0.78	1.25	0.75
$S + SH = S_2 + H$	1.11	3.00	0.63
$H + HSS = SH + SH$ (1)	2.82	3.00	0.67
$H + HSS = SH + SH$ (2)	1.35	3.00	1.22
$SH + SH$ (+M) = HSSH	0.17	0.17	1.55
Low pressure limit	3.00	1.11	1.50
$SH + HSS = H_2S + S_2$	0.33	0.33	1.11
$H_2S + S$ (+M) = HSSH (+M)	0.63	0.39	2.00
$SH + HO_2 = H_2S + O_2$	1.35	1.35	0.84
$H_2S + O = SH + OH$	0.50	0.77	2.00
$S + O_2 = SO + O$	0.90	0.80	1.10
$SO + O_2 = SO_2 + O$	0.89	0.89	0.84
$H + SO_2$ (+M) = HOSO (+M)	1.50	1.20	0.33
Low pressure limit	1.89	0.81	0.35
$S_2 + O = SO + S$	1.20	1.35	1.68

10
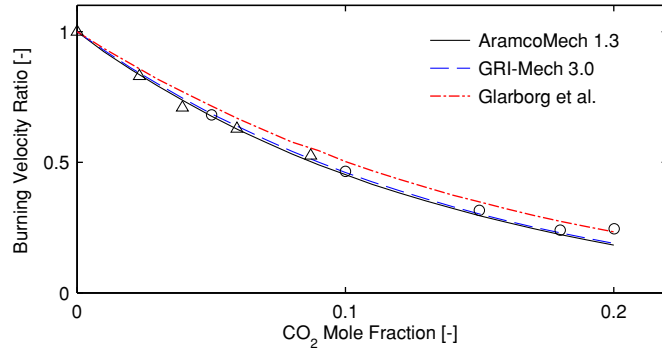
Figures

Figure 1: The modeling results (lines) agree well with the experimental data (symbols) of Halter et al. [20] (○) and Kishore et al. [21] (△) on the reduction of the laminar burning velocity of stoichiometric CH_4-air flames through CO_2 addition (T = 300 K, p = 1 atm).
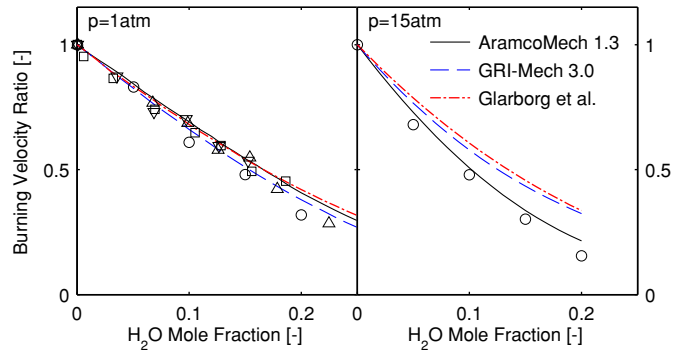
Figure 2: The modeling results (lines) agree well with the experimental data (symbols) of Albin et al. [22] (△,▽), Mazas et al. [23] (□), and Babkin and V'yun [24] (○) on the reduction of the laminar burning velocity of stoichiometric CH_4-air flames through H_2O addition at atmospheric pressure (a). At high pressure, AramcoMech 1.3 preforms better than the other mechanisms (b).
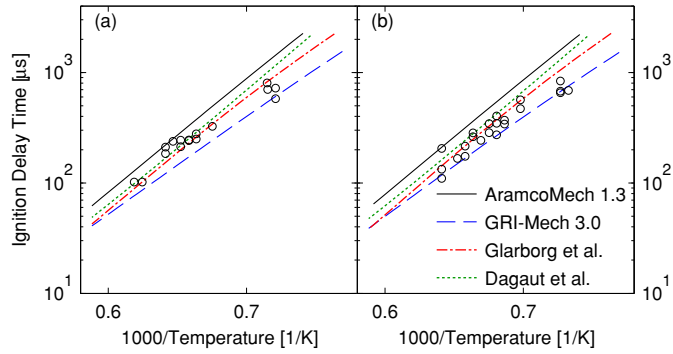
Figure 3: The modeling results (lines) agree well with the experimental data (symbols) of Levy et al. [26] on the ignition delay time of CH_4 at p = 7-9 bar, Φ = 0.3. (a) N_2 dilution with 5.2% CO_2, (b) N_2 dilution with 5.2% CO_2 and 4.0% H_2O.
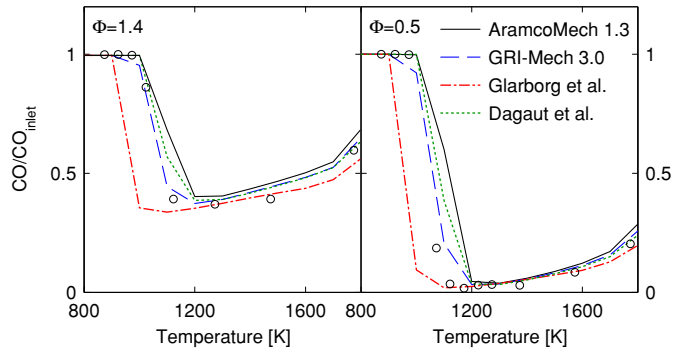
Figure 4: Comparison between modeling results (lines) and data (symbols) from the atmospheric $CO/O_2/CO_2/H_2O/N_2$ flow reactor of Abián et al. [27]. The modeling was done assuming plug flow with a flow rate of 1 l_{STP}/min and the temperature profiles given in [63]. Inlet conditions: $X_{CO} \approx 2000$ ppm, X_{H_2O} = 0.6%, X_{CO_2} = 75%, balance N_2.
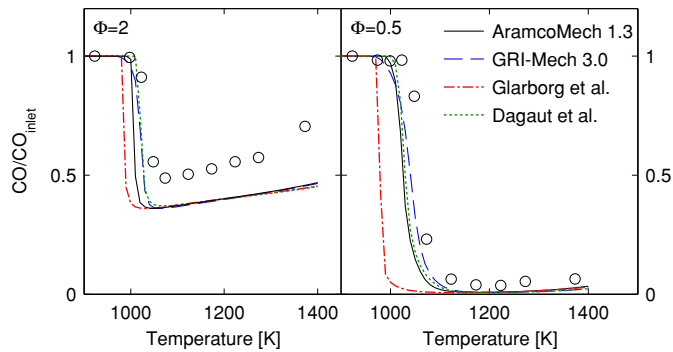
Figure 5: Comparison between modeling results (lines) and data (symbols) from the atmospheric $CO/O_2/CO_2/H_2O/N_2$ flow reactor of Abián et al. [27]. Inlet conditions: $X_{CO} \approx 5100$ ppm, X_{CO_2} = 25%, X_{H_2O} = 10%, balance N_2.
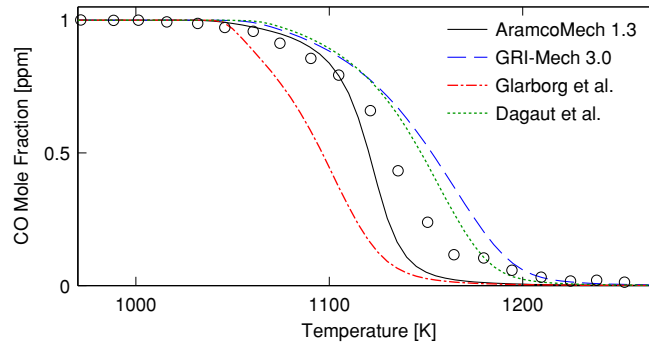
Figure 6: Comparison between modeling results (lines) and data (symbols) from the atmospheric flow reactor experiment of Glarborg et al. [28]. No full experimental temperature profiles were available so that a fixed residence time of $\tau = 64/T$ s was assumed, where T is the constant reactor temperature in kelvin. Inlet conditions: $X_{CO} \approx 1500/1630$ ppm, $X_{O_2} = 2.0\%$, $X_{O_2} = 32.0\%$, balance N_2.
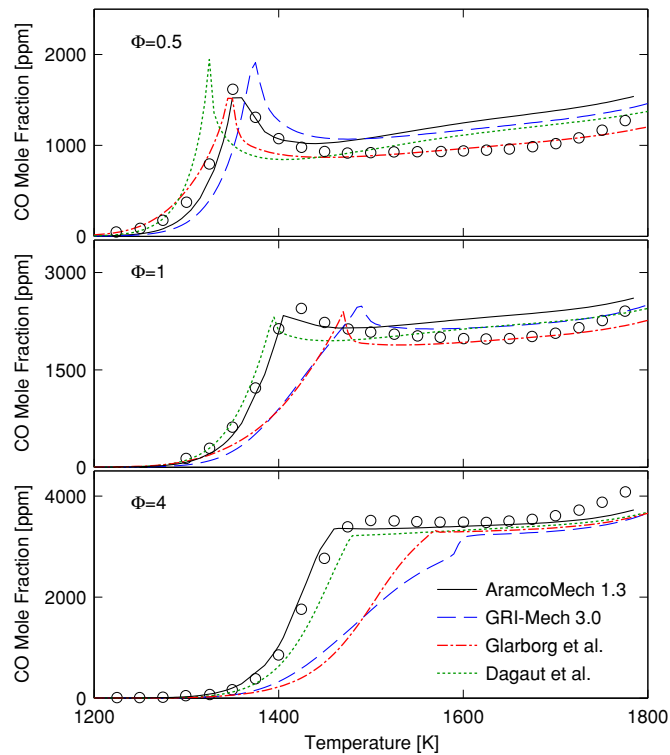
Figure 7: Comparison between modeling results (lines) and data (symbols) from the atmospheric $CH_4/O_2/CO_2/N_2$ flow reactor of Glarborg and Bentzen [8] on CO formation in CH_4 oxidation in the presence of CO_2. The modeling was done assuming a residence time of $\tau \approx 960/T$ s and constant temperature. Inlet conditions: $X_{CO} \approx 1000$ ppm, $X_{CO_2} = 77\text{-}95$ %, balance N_2.
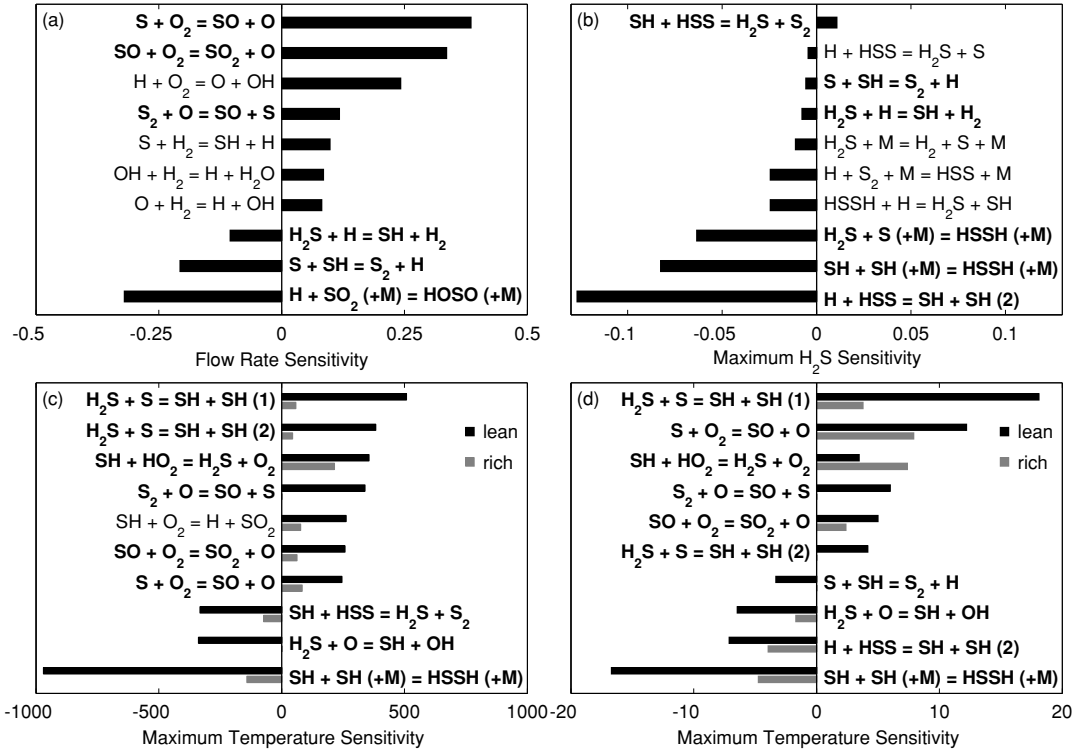
Figure 8: Sensitivity coefficients of the pre-exponential factor of different reactions. (a) Sensitivity with respect to the laminar burning velocity of H_2S in air at $p = 1$ atm, $\Phi = 1$; (b) Sensitivity with respect to the H_2S concentration in the pyrolysis experiment [43] at $T = 1000$ °C; (c) Sensitivity with respect to temperature in the ignition delay measurement [29] for $T_0 = 950$ K; (d) Sensitivity with respect to temperature in the ignition delay measurement [29] for $T_0 = 1200$ K.
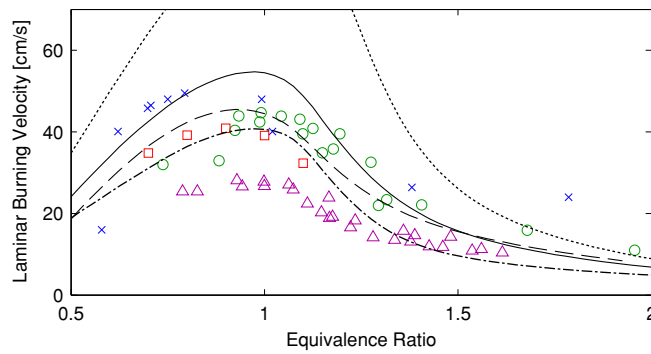
Figure 9: Laminar burning velocity of H_2S in air at atmospheric pressure. The symbols are the experimental data of Chamberlin and Clarke [39] (×), Cohen [40] (○), Gibbs and Calcote [41] (□), and Flockenhaus [42] (△). The lines are results of the present modeling study: Basic mechanism (solid), Optimization 1-12 (dashed), Optimization 1-7 (dash-dotted), Optimization 8-12 (dotted). Both Soret effect and multicomponent diffusion were used for the modeling.
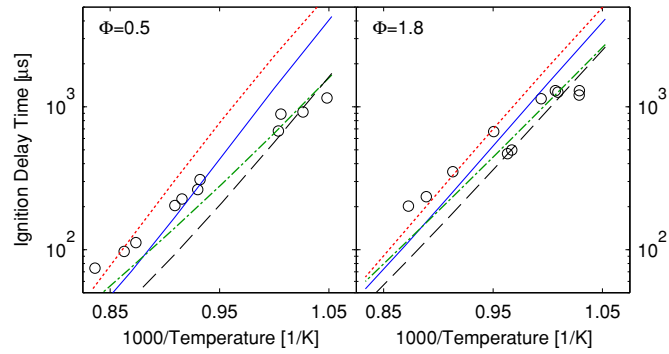
Figure 10: Ignition delay time of H_2S in air as a function of temperature. The symbols are the experimental data of Frenklach et al. [29]. The lines are results of the present modeling study: Basic mechanism (solid), Optimization 1-12 (dashed), Optimization 1-7 (dash-dotted), Optimization 8-12 (dotted). P = 30-45 atm. The pressure was varied along with the initial temperature to keep the partial density of H_2S constant.
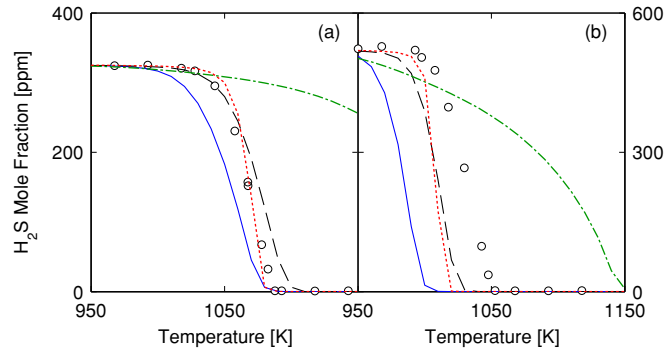
Figure 11: Comparison between the experimental data (symbols) for the atmospheric $H_2S/O_2/N_2$ flow reactor of Zhou et al. [35] and the results of the present modeling study: Basic mechanism (solid), Optimization 1-12 (dashed), Optimization 1-7 (dash-dotted), Optimization 8-12 (dotted). The modeling was done using temperature profiles similar to the one shown in [35]. Inlet conditions: (a) X_{H_2S} = 325 ppm, X_{O_2} = 600 ppm; and (b) X_{H_2S} = 520 ppm, X_{O_2} = 1000 ppm.
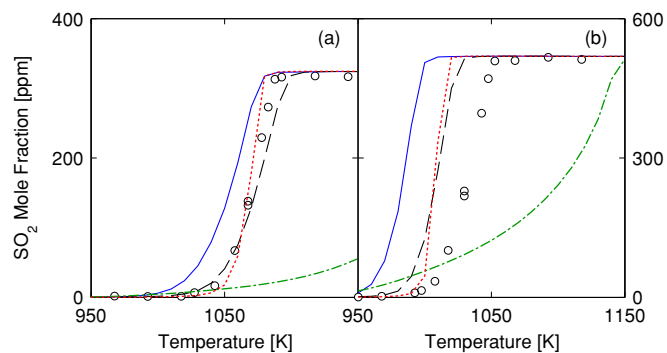
Figure 12: Comparison between the experimental data (symbols) for the atmospheric $H_2S/O_2/N_2$ flow reactor of Zhou et al. [35] and the results of the present modeling study: Basic mechanism (solid), Optimization 1-12 (dashed), Optimization 1-7 (dash-dotted), Optimization 8-12 (dotted). Same conditions as in Fig. 11.

15
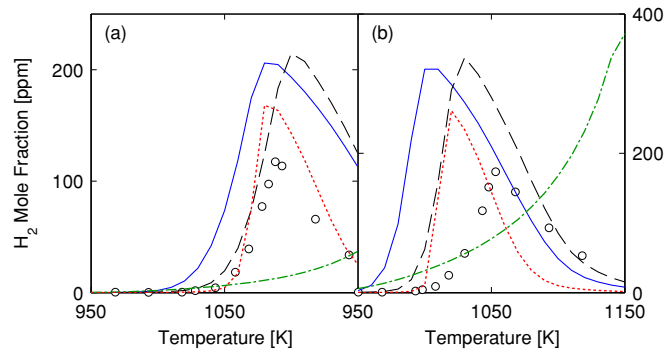
Figure 13: Comparison between the experimental data (symbols) for the atmospheric $H_2S/O_2/N_2$ flow reactor of Zhou et al. [35] and the results of the present modeling study: Basic mechanism (solid), Optimization 1-12 (dashed), Optimization 1-7 (dash-dotted), Optimization 8-12 (dotted). Same conditions as in Fig. 11.
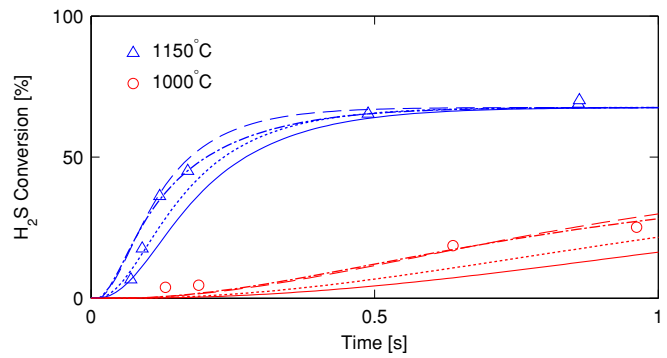
Figure 14: Comparison between modeling results (lines) and experimental data (symbols) of Hawboldt et al. [43] for the pyrolysis of H_2S at atmospheric pressure. Basic mechanism (solid), Optimization 1-12 (dashed), Optimization 1-7 (dash-dotted), Optimization 8-12 (dotted). Initial conditions: $X_{H_2S} = 2.5\%$, balance N_2.

16
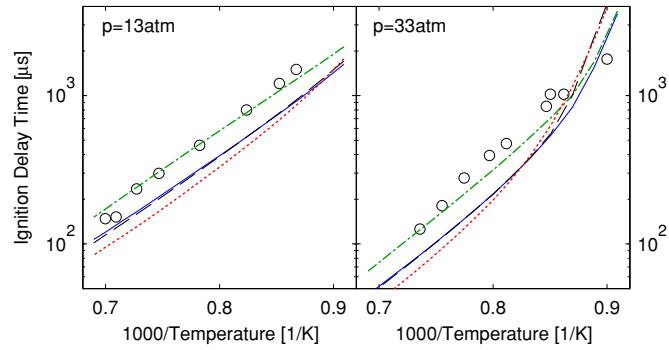
Figure 15: Ignition delay time of H_2/H_2S mixtures in Ar at different pressures. The symbols are the experimental data of Mathieu et al. [56]. The lines are results of the present modeling study: Basic mechanism (solid), Optimization 1-12 (dashed), Optimization 1-7 (dash-dotted), Optimization 8-12 (dotted). Initial conditions: X_{H_2} = 1%, X_{O_2} = 1%, X_{H_2S} = 0.16%, balance Ar.
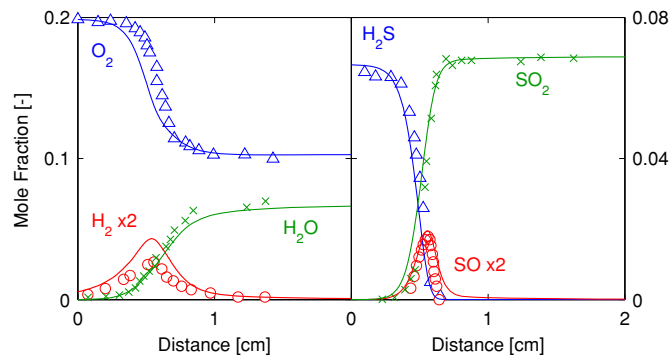
Figure 16: Comparison between modeling results (lines) and experimental data (symbols) for the H_2S-air flame of Merryman and Levy [57]. P = 0.1 atm, Φ = 0.5. Plot was divided for better readability. The modeling used the experimental temperature profile and extrapolated upstream to 300 K.
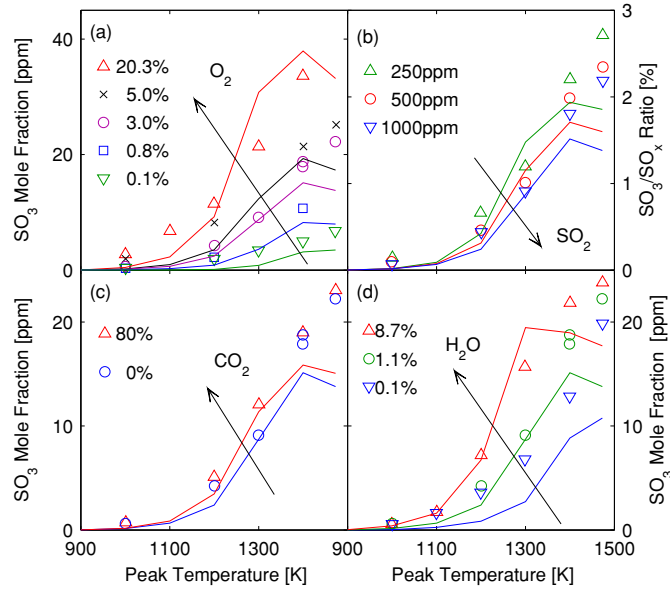
Figure 17: Comparison between modeling results (lines) and experimental data (symbols) for the atmospheric flow reactor of Fleig et al. [62]. The modeling was done for a fixed flow rate of 1.011 l_{STP}/min using the experimental temperature profiles. Inlet conditions: (a) X_{SO_2} = 1000 ppm, X_{H_2O} = 1.11%, varying O_2; (b) X_{O_2} = 3%, X_{H_2O} = 1.11%, varying SO_2; (c) X_{SO_2} = 1000 ppm, X_{O_2} = 3%, X_{H_2O} = 1.11%, varying CO_2; (d) X_{SO_2} = 1000 ppm, X_{O_2} = 3%, varying H_2O. Balance N_2 in all cases.
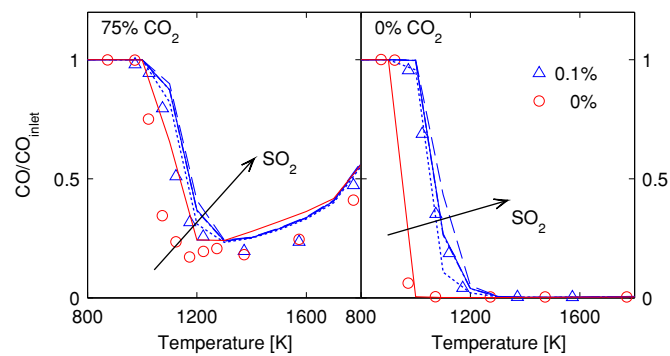
Figure 18: Comparison between modeling results (lines) and experimental data (symbols) for the atmospheric flow reactor of Giménez-López et al. [63]. The modeling was done at a constant flow rate of 16.7 cm^3_{STP}/s using the measured temperature profile. Inlet conditions: X_{CO} = 2000 ppm, X_{O_2} = 1000 ppm, X_{H_2O} = 0.6%, X_{CO_2} = 75%/0%, varying SO_2, balance N_2.

18
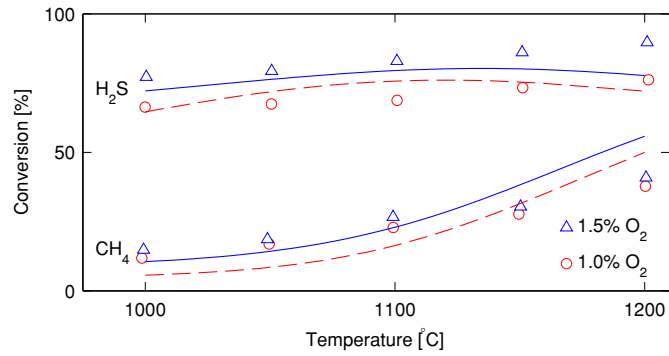
Figure 19: Comparison between modeling results (lines) and experimental data (symbols) for the flow reactor of Chin et al. [65]. $P = 1.1$ bar. Inlet conditions: $X_{H_2S} = 2.45\%$, $X_{CH_4} = 2.45\%$, varying O_2, balance N_2; $\tau = 0.6$ s.
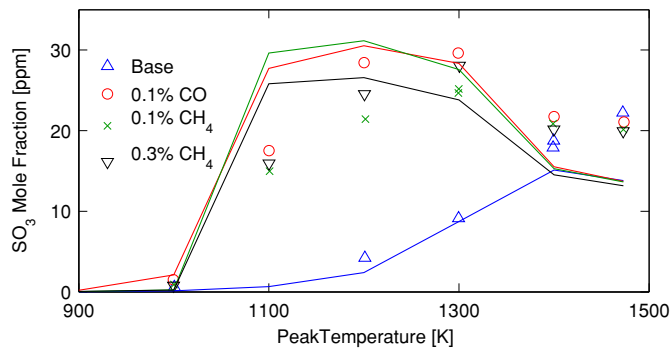
Figure 20: Comparison between modeling results (lines) and experimental data (symbols) for the atmospheric flow reactor of Fleig et al. [62]. Inlet conditions: $X_{SO_2} = 1000$ ppm, $X_{O_2} = 3\%$, $X_{H_2O} = 1.11\%$, varying CO and CH_4, balance N_2.

19